Proceedings of Montreal 2018
Global Power and Propulsion Forum
7th – 9th May, 2018
www.gpps.global

GPPS-NA-2018-0123

COMPARISON OF EXPERIMENTS, FULL-ANNULUS-CALCULATIONS AND HARMONIC-BALANCE-CALCULATIONS OF A MULTI-STAGE COMPRESSOR

Oliver K. Reutter
DLR, German Aerospace Center
Institute of Propulsion Technology
Oliver.Reutter@dlr.de
Cologne, Germany

Graham Ashcroft
DLR, German Aerospace Center
Institute of Propulsion Technology
Graham.Ashcroft@dlr.de
Cologne, Germany

Eberhard Nicke
DLR, German Aerospace Center
Institute of Propulsion Technology
Eberhard.Nicke@dlr.de
Cologne, Germany

Edmund Kuegeler
DLR, German Aerospace Center
Institute of Propulsion Technology
Edmund.Kuegeler@dlr.de
Cologne, Germany

ABSTRACT

The 4.5 stage DLR research compressor Rig250, which is representative of the front stages of a modern high pressure compressor, has been investigated experimentally and numerically. In order, to enable comparisons with the time-resolved experimental data both steady and unsteady numerical simulations have been performed. In these simulations, both time- and frequency-domain methods have been employed.

For the time-domain calculations the model consisted of the full annulus mesh of the first two stages including the IGVs and struts located upstream in a swan neck. In total, the mesh has about $1x10^9$ nodes and is distributed over 6000 blocks.

For the frequency-domain calculations the Harmonic Balance (HB) method has been used. By exploiting the spatial and temporal periodicity of the configuration the HB method only requires a single passage to be resolved per blade row, thus significantly reducing the mesh size and calculation time.

In this work the results of the time- and frequency-domain simulations are compared with each other and the available steady and unsteady experimental data. In particular, the importance of selecting the appropriate Fourier modes and the challenge this presents in multistage configurations is emphasized. The drawbacks and advantages of the two numerical methods are discussed.

INTRODUCTION

The DLR compressor Rig250 has been investigated numerically and experimentally. It is representative of the first stages of a high pressure compressor used in jet engines or stationary gas turbines. It consists of 4.5 stages and struts located in a swan neck. Figure 1 shows the blade row numbers of Rig250.

As investigations become more and more detailed, it is becoming ever more important to simulate also time-dependent behaviour of compressors. These unsteady calculations can either be conducted in the time-domain or in the frequency-domain. The time-domain calculations have the drawback of being very resource consuming. In the frequency-domain the meshes are much smaller, but much more care has to be given to the set-up for choosing, which frequencies are included in the model.

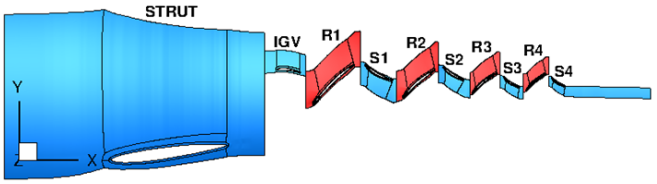

BLADE ROW:	STRUT	IGV	R1	S1	R2	S2	R3	S3	R4	S4
BLADE COUNT:	7	40	23	36	28	48	38	68	47	80

Figure 1 Blade rows and counts of Rig250

EXPERIMENTAL SET-UP

The DLR Rig250 is a heavily instrumented research compressor. In Figure 2, a cut through the Rig250 is depicted. IGV, Stator1, and Stator2 are adjustable for start-up and part-speed operation. In the here investigated case at 100 % nominal speed all variable vanes are in their nominal settings. There are, including all sensors necessary for operation nearly 1000 sensors which measure pressure, temperature, strain, mass flow and speed. Some of the pressure sensors are dynamic pressure sensors with a sampling rate of 40 kHz. Most sensors record one sample per second and thereby deliver steady state measurements. The experiment is conducted at the M2VP test facility at DLR in Cologne.

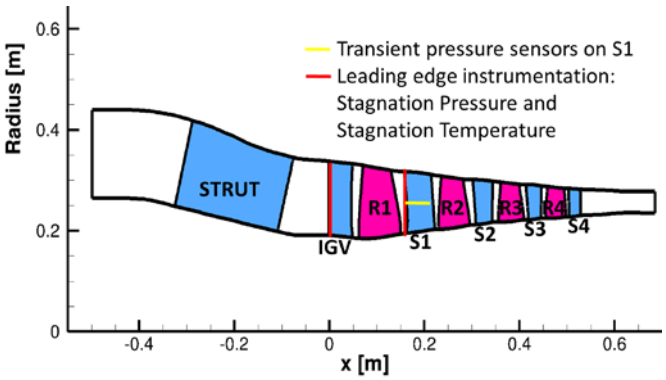

Figure 2 Instrumentation of Rig250 in meridional view

The Compressor Test Facility (M2VP)

The experimental investigations were conducted at the DLR Cologne compressor test facility (M2VP), shown in Figure 3 and Figure 4. The outlet equipped with a fan is an option for test of fans with low pressure ratios and high mass flows and is not used for tests of Rig250.

The facility comprises two 5 MW electrical motor drives with a flexible gearbox system, see Figure 4 a and b. For the investigations in this work both motor drives were combined through a coupling system. In this case the drive shaft speed is limited to 20.000 rpm. The rig tests were carried out in an open loop configuration, meaning that ambient air was sucked through a tower (left in Figure 4 c), a settling chamber and a bell mouth before arriving to the compressor.

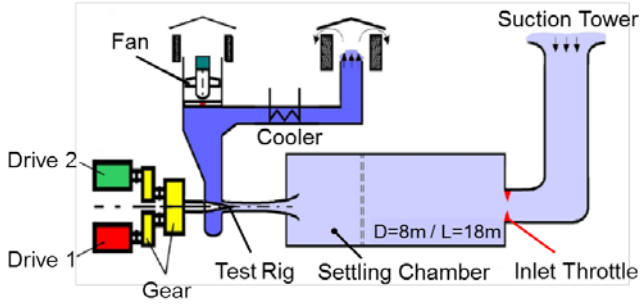

Figure 3 Overview of the M2VP test facility

The distance between the settling chamber (18 m long and 6 m in diameter) and the inlet of the compressor is sufficiently large so that disturbances in the inflow can become homogenized. The air passes through the rig and is throttled by a ring throttle at the rear. The compressed, hot air leaves the test bed into the atmosphere via exit pipes with an integrated cooler (exhaust – at the right side in Fig. 5c). As the power is not sufficient to run the Rig250 at design rotational speeds a throttle at the settling chamber entry is used to limit the total pressure in the chamber to about 80 kPa.

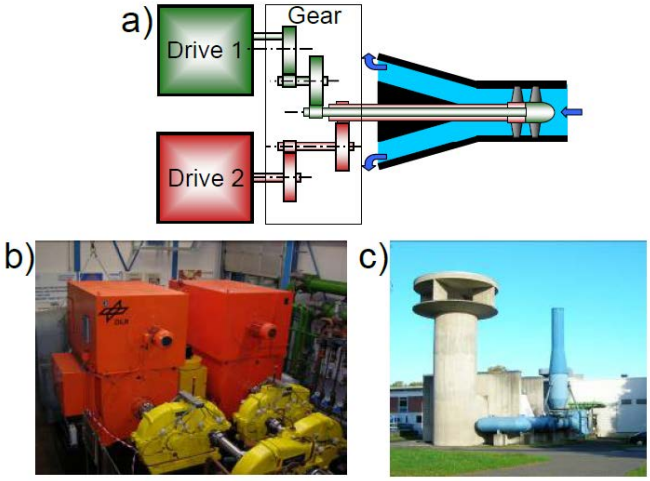

Figure 4 Multistage Two Shaft Compressor Test Facility with a) rotor system with hollow shaft and core, b) drive motors (orange) and gear boxes (yellow), c) test building with air suction tower (grey, left) and exhaust (blue, right)

Instrumentation

The instrumented Rig 250 is shown in Figure 5. Here, the many pressure tabs, instrumentation cables and their connection to the data acquisition system can be seen.

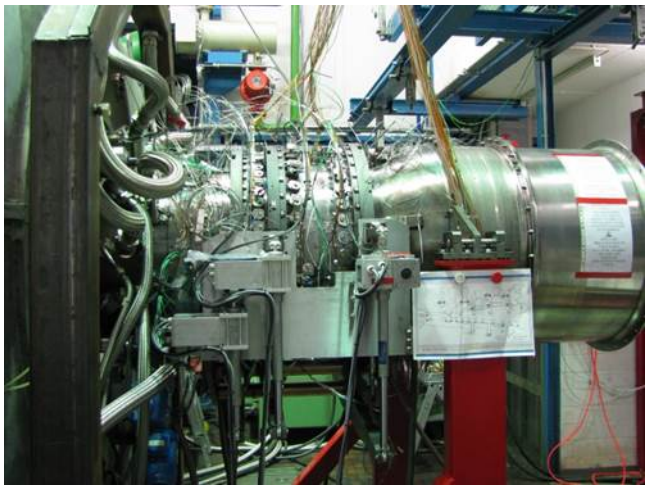

Figure 5 Picture of the instrumented Rig250

Of the many sensors in Rig250, a special emphasis is put on the transient measurements on mid-span Stator1 in this

paper for analysation. At the time of the experiment there were two sensors on the pressure side of vane 23 and four sensors on the suction side of vane 24 still working and recorded reasonable measurement data. An overview of the location of the sensors in the meridional plane is given in Figure 2. On the full annulus 4 to 12 vanes of each stator row were equipped with sensors.

NUMERICAL SET-UP TIME-DOMAIN

In order to keep the model within the capacity of the computer cluster of the institute the model did not consist of the entire compressor as a full annulus model. So in the calculations described here the first 6 rows were represented by a full annulus low-Reynolds mesh, whereas the last 4 rows were added as single passage steady calculations, resulting in 186 calculated blades. The last two stages as single passages served to obtain the time mean flow in order to set the boundary conditions for the time accurate calculations. Care was taken to have y+ values of 1 and smaller on all wetted surfaces. Consequently, low-Reynolds boundary conditions are used on all solid walls. The resulting mesh had nearly 1 billion nodes distributed over 6000 structured blocks. The computational mesh was created using DLR's in-house, block-structured meshing tool PyMesh (Weber and Sauer, 2016). The mesh uses only structured hexahedral elements. Care is taken to avoid large stretching and skewness.

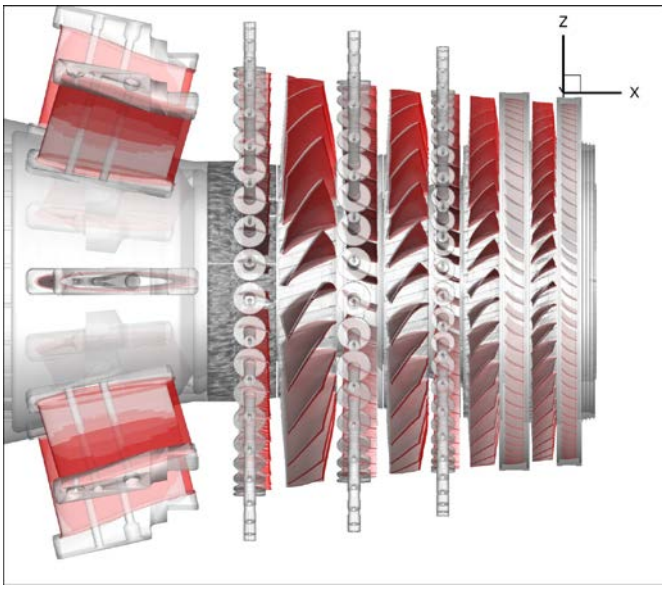

Figure 6 CAD model (grey) and CFD model (red) of Rig250 (Reutter et al., 2017)

In Figure 6 the blades of the CFD model are depicted in semi-transparent red on top of a semi-transparent grey CAD model. The blades in the numerical model are positioned in the same positions as in the experiment. The importance of this positioning can for example be seen in the detailed analysis of the experimental and numerical wake of the strut (Reutter et al., 2017).

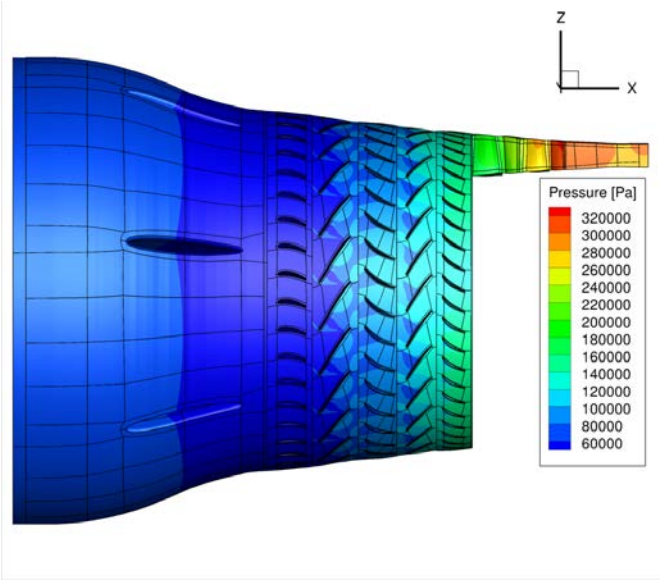

Figure 7 Numerical set-up of Rig250 showing the static pressure distribution

As the RANS- solver the DLR-solver TRACE was used. TRACE is developed at DLR especially for turbo machinery applications (Becker et al., 2010, Franke et al., 2010). It has been used and validated in many different turbo machinery projects.

In Figure 7 the numerical set-up is shown. The block borders are drawn, so that the extensive splitting can be seen, which is necessary to divide the numerical tasks onto 1200 processor cores. Also one sees, that the first six rows starting from the strut up to Stator2 are calculated in full annulus unsteady Reynolds-averaged Navier-Stokes (RANS) calculations, whereas the last 4 rows (Stage 3 and stage 4) are added in single passage steady RANS calculations. In the first 6 rows zonal connections between the rows, in the last 4 rows mixing-planes were used. An implicit, second-order accurate backward difference formula (BDF2) was used. As the turbulence model the two equation k-ω model by Wilcox is used (Wilcox, 1988). Extensions for stagnation point anomaly by the Kato-Launder approach (Kato and Launder, 1993), for rotational effects by the approach of Bardina (Bardina et al., 1985) and for compressible effects are used. At the calculated rotational speed of 12720 rpm the calculations used 1536 time-steps per wheel rotation, corresponding to 32 time-steps per Vane Passing Frequency (VPF) in Rotor2's frame of reference and consequently disturbances with frequencies up to 10176 Hz are resolved. The limited accuracy of BDF2 method does not allow the flow unsteadiness to be accurately resolved beyond this frequency. The transient RANS calculations used a converged steady calculation on the same mesh as initialization.

The boundary conditions were taken from the experiment, with profiles of total temperature and total pressure, together with the radial and circumferential flow angles prescribed at the inlet. At the outlet static pressure is used as the boundary condition for the calculations. The

time-accurate, unsteady simulations were started from a converged steady-state simulation.

The set-up file used about 108 GB of disk storage space. Even though this file contains two time-steps to allow a good restart, it was by no way possible within the available disk capacity to save a full revolution of the entire set-up. Therefore all experimental probe positions were transferred into the numerical set-up. A mesh node can be set to be a probe position and then every time-step for this node all physical values are written into a file. So for all experimental probes numerical probes were added. Due to the long run times and the computational costs of the calculation only one run was possible and mistakes in the list of numerical probes cannot be changed after starting. Additionally after one revolution an average file is written, which contains the mean values of the solution.

The calculation took 10 days on 1200 cores for one revolution. About 3 revolutions were calculated.

NUMERICAL SET-UP FREQUENCY-DOMAIN

Alongside conventional time-domain based steady and unsteady modules the TRACE code also includes a Harmonic Balance (HB) module (Frey, et al. 2014). As an alternating time/frequency-domain method the Harmonic Balance solver in TRACE requires the solution harmonics to be specified explicitly in terms of frequency and inter-blade phase angle. Unfortunately, and in particular for large multistage configurations, it is not always immediately clear which solution harmonics are going to be relevant. For the HB simulations presented in this work two basic sets of solution harmonics have been considered. The first set of solution harmonics, listed in Table 1, includes only those harmonics generated by the interaction of a given blade row with its immediate neighbors.

Table 1 Solution Harmonics – Baseline

Strut	Base Mode	$(0,N_{IGV})$	
	Harmonics	0 1 2 3	
IGV	Base Mode	$(0,N_{Strut})$	(BPF_{R1},N_{R1})
	Harmonics	0 1 2 3 4 5 6	0 1 2 3
R1	Base Mode	(VPF_{IGV},N_{IGV})	(VPF_{S1},N_{S1})
	Harmonics	0 1 2 3	0 1 2 3
S1	Base Mode	(BPF_{R1},N_{R1})	(BPF_{R2},N_{R2})
	Harmonics	0 1 2 3	0 1 2 3
R2	Base Mode	(VPF_{S1},N_{S1})	(VPF_{S2},N_{S2})
	Harmonics	0 1 2 3	0 1 2 3
S2	Base Mode	(BPF_{R2},N_{R2})	(BPF_{R3},N_{R3})
	Harmonics	0 1 2 3	0 1 2 3
R3	Base Mode	(VPF_{S2},N_{S2})	(VPF_{S3},N_{S3})
	Harmonics	0 1 2 3	0 1 2 3
S3	Base Mode	(BPF_{R3},N_{R3})	(BPF_{R4},N_{R4})
	Harmonics	0 1 2 3	0 1 2 3
R4	Base Mode	(VPF_{S3},N_{S3})	(VPF_{S4},N_{S4})
	Harmonics	0 1 2 3	0 1 2 3
S4	Base Mode	(BPF_{R4},N_{R4})	
	Harmonics	0 1 2 3	

Table 2 Solution Harmonics – Extended Configuration

Strut	Base Mode	$(0,N_{IGV})$					
	Harmonics	0 1 2 3					
IGV	Base Mode	$(0,N_{Strut})$	(BPF_{R1},N_{R1})				
	Harmonics	0 1 2 3…10	0 1 2 3				
R1	Base Mode	(VPF_{IGV},N_{IGV})	(VPF_{S1},N_{S1})	(VPF_{Strut},N_{Strut})			
	Harmonics	0 1 2 3 4 5 6	0 1 2 3	0 1 2 3...10			
S1	Base Mode	(BPF_{R1},N_{R1})	(BPF_{R2},N_{R2})	$(0,N_{IGV})$	$(BPF_{R1},-N_{IGV}-N_{R1})$		
	Harmonics	0 1 2 3	0 1 2 3	0 1 2 3	0 1		
R2	Base Mode	(VPF_{S1},N_{S1})	(VPF_{S2},N_{S2})	$(0,N_{R1})$	$(VPF_{S1},-N_{R1}-N_{S1})$	$(VPF_{S1},-2N_{R1}-N_{S1})$	
	Harmonics	0 1 2 3	0 1 2 3	0 1 2 3	0 1	0 1	
S2	Base Mode	(BPF_{R2},N_{R2})	(BPF_{R3},N_{R3})	$(0,N_{S1})$	$(BPF_{R2},-N_{R2}-N_{S1})$		
	Harmonics	0 1 2 3	0 1 2 3	0 1 2	0 1		
R3	Base Mode	(VPF_{S2},N_{S2})	(VPF_{S3},N_{S3})	$(0,N_{R2})$	$(VPF_{S2},-N_{R2}-N_{S2})$	$(VPF_{S2},-2N_{R2}-N_{S2})$	$(VPF_{S2},-3N_{R2}-N_{S2})$
	Harmonics	0 1 2 3	0 1 2 3	0 1 2 3	0 1	0 1	0 1
S3	Base Mode	(BPF_{R3},N_{R3})	(BPF_{R4},N_{R4})	$(0,N_{S2})$	$(BPF_{R3},N_{S2}+N_{R3})$		
	Harmonics	0 1 2 3	0 1 2 3	0 1 2 3	0 1		
R4	Base Mode	(VPF_{S3},N_{S3})	(VPF_{S4},N_{S4})	$(0,N_{R3})$	$(VPF_{S3},-N_{R3}-N_{S3})$	$(VPF_{S3},-2N_{R3}-N_{S3})$	
	Harmonics	0 1 2 3	0 1 2 3	0 1 2 3	0 1	0 1	
S4	Base Mode	(BPF_{R4},N_{R4})	$(0,N_{R3})$	$(VPF_{S3},N_{S3}-2N_{R4}$	$(VPF_{S3},N_{S3}+N_{R3})$		
	Harmonics	0 1 2 3	0 1 2 3	0 1	0 1		

Consequently, in each blade row, we have two harmonic sets: one arising from the interaction with the upstream blade row and one arising from the interaction with the downstream blade row. To resolve these effects the first four harmonics (0-3) of each fundamental mode have been included in each blade row. As an exception to this rule

seven harmonics (0-6) have been included in the IGV to resolve the strut's wake. Here a larger number of harmonics was selected both due to the very low number of struts and their narrow wake structures.

A second and extended set of solution harmonics was created following a preliminary analysis of the baseline configuration. The aim of extending the set of solution harmonics was to include interaction effects between non-adjacent blades, e.g. blade-to-blade indexing. In addition, in an attempt to resolve the strut wake in the IGV, the number of solution harmonics was raised to eleven (0-10). The extended set of solution harmonics is shown in Table 2.

To determine which additional modes to include in the extended configuration an analysis of the results of the baseline configuration was performed. In particular, an analysis of the circumferential modes of each solution harmonic was performed and the dominant modes identified. Example results of this analysis are shown below in Figure 8.

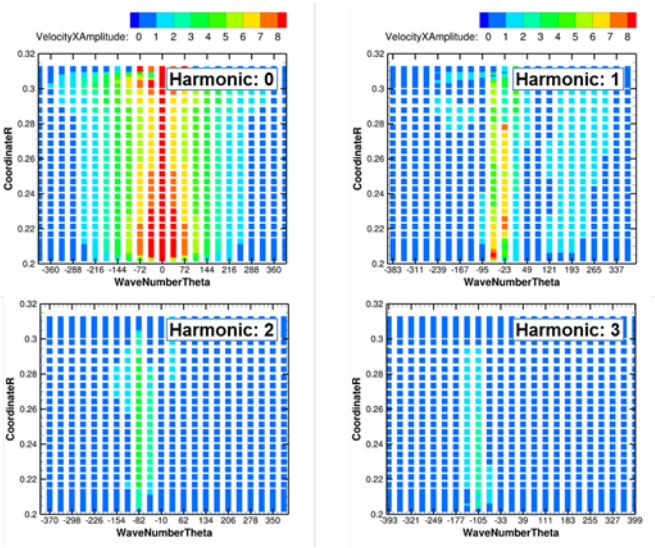

Figure 8 Modal analysis at the interface between S1 and R2

Here, for the four solution harmonics at the interface between S1 and R2, the distribution of energy over the circumferential wavenumbers and between hub and tip is shown in terms of the amplitude of the fluctuations in axial velocity. For the zeroth harmonic it can be seen that the modes 0, ±36, ±72 are dominant. These modes describe the wake of stators S1 and are simply multiples of the blade count (N_{S1}). For the first higher harmonic the modes -23 and -59 are dominant. The first of these modes corresponds to the first harmonic of the rotor R1 ($-N_{R1}$). In contrast the second mode is due to the interaction (scattering) of the rotor R1 wake with the stators in the S1 blade row. In the second and third harmonics the modes -82 and -105 are dominant. With the dominant spatial modes identified, the necessary solution harmonics required in the adjacent blade rows to capture these modes are computed using the transformation rule

$$\omega' = |\omega + m(\Omega' - \Omega)|$$

As the HB solver repeatedly transforms between the time- and frequency domains it also necessary to specify the number of sampling points to resolve a harmonic in the time-domain and consequently use to compute the discrete Fourier transform of the nonlinear residual. In this work five sampling points have been used for the highest harmonics.

RESULTS AND DISCUSSION

Comparison of Extended and Baseline HB Models

To provide qualitative overview of the impact of the additional solution modes in the extended HB setup, Figure 9 shows a comparison of the computed flow fields at midspan in terms of instantaneous snapshots of the entropy field. Compared with the results obtained with the baseline setup (Figure 9a), it can be seen that the additional modes included in the extended setup allow the rotor-rotor and stator-stator interaction effects to be captured (Figure 9b). Furthermore, as desired, the strut wake is more accurately compact in the IGV blade row.

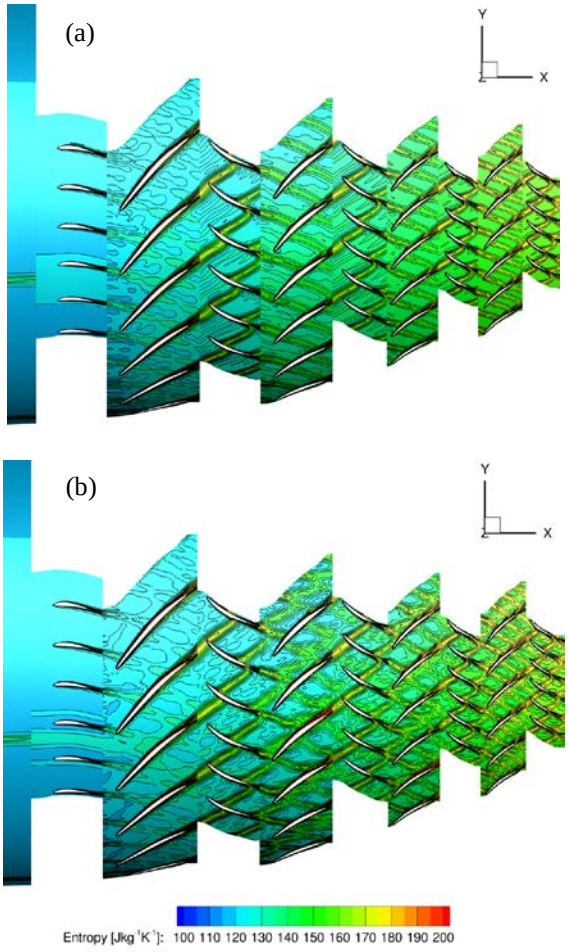

Figure 9 Comparison of Baseline and Extended HB Models: Instantaneous snapshots of entropy.

Comparison at the IGV

Starting from the inlet the flow first passes the struts and the IGVs. The stagnation pressure instrumentation of the IGV steady results shows good agreement between experimental and full annulus time-domain calculations, as reported in Reutter et al., 2017, see Figure 10.

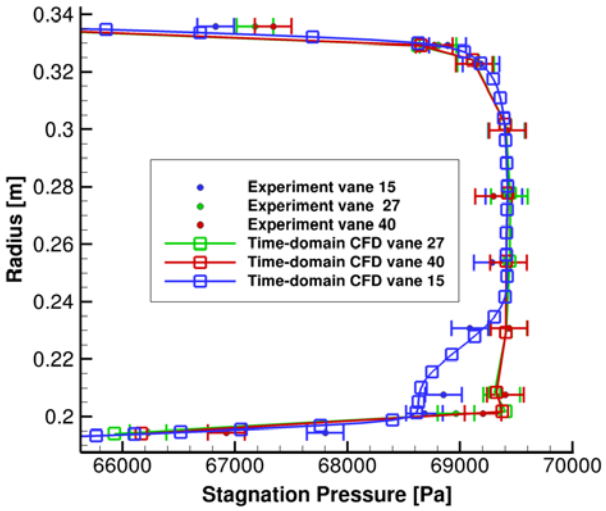

Figure 10 Comparison of experimental and time-domain full annulus results (adapted from Reutter et al., 2017)

As explained there the strut wake is rather narrow and therefore exact positioning of the sensor is of great importance.

While this detail can be reproduced in the full annulus calculations it is not feasible to match the sensors affected by the strut wake with the results from the frequency-domain calculations. Even when using up to 10 harmonics, the wake of the strut is not resolved sufficiently to be able to match the full annulus calculations or the experimental results. The difficulty is that there are only seven struts with rather small, sharply distinct wakes on the full annulus, so that so many harmonics would have to be used, that there is no advantage any more compared to the full annulus calculation concerning effort, see Figure 11.

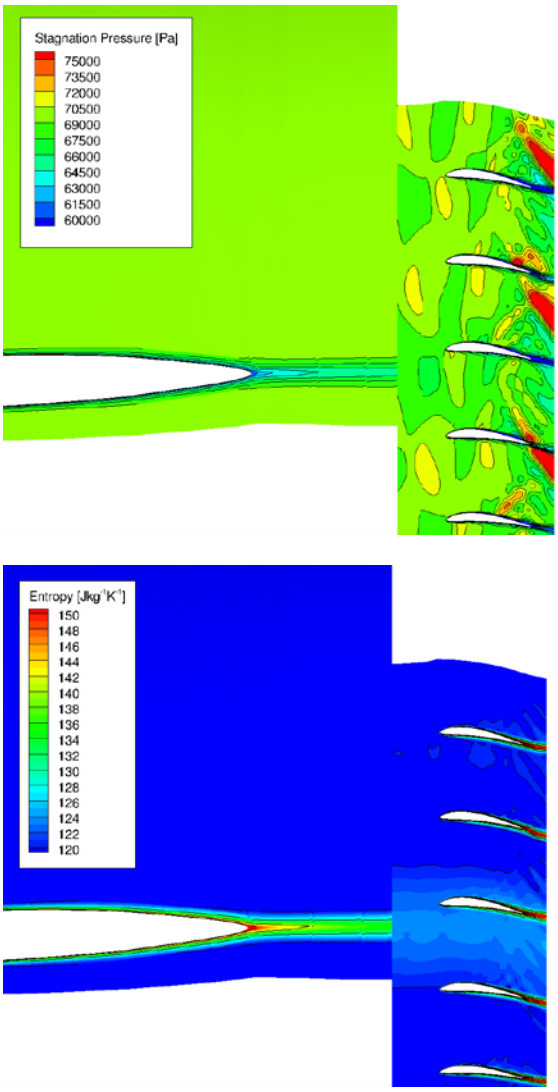

Figure 11 The strut-IGV interaction in the frequency-domain calculation: Stagnation pressure (above) and entropy (below)

The time-domain calculations show that the transfer of information between rows is larger than in the frequency-domain calculations. The wake of the strut is clearly transported through the IGV into Rotor1. Figure 13 shows a detail, marked by the rectangle in Figure 12 above, where the lower IGV is fully hit by a strut wake and therefore exhibits a larger wake which is transported to Rotor1. Even this stronger wake does not affect the shock position notably. In this figure also the small shifts and deviations along the zone border from the non-moving IGV mesh to the moving Rotor1 mesh can be seen when looking closely. Care has been taken to keep mesh resolutions in all rows similar to make these numerical effects as small as possible.

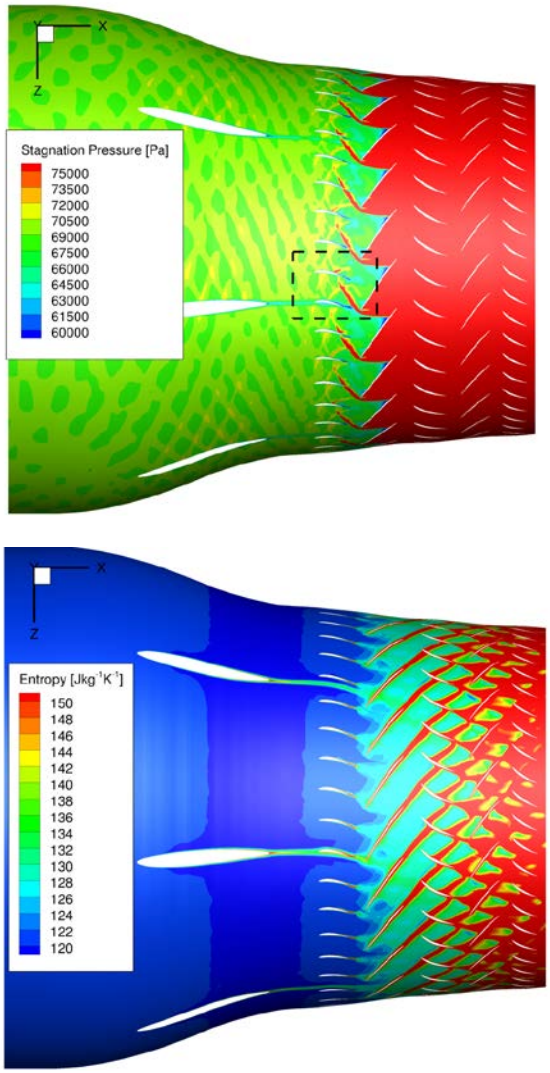

Figure 12 Full annulus calculation in the time-domain: Stagnation pressure (above) and entropy (below) and at 88 % span

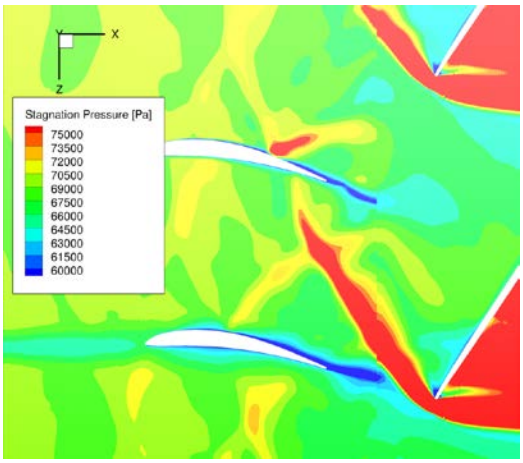

Figure 13 Detail from of the IGV-Rotor1 interaction

Comparison at Stator1

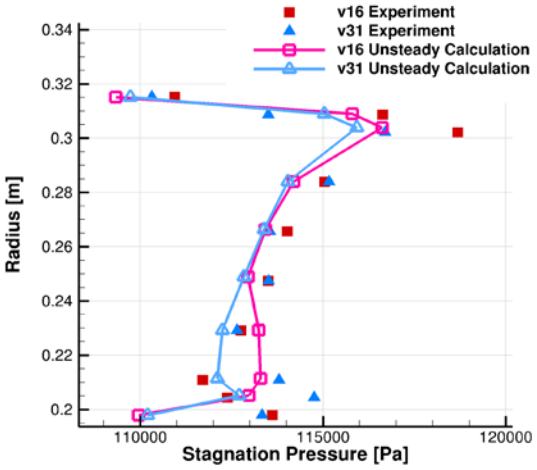

Figure 14 Stagnation pressure at the leading edge of Stator1 for two instrumented vanes

The comparison between probes at the leading edge of Stator1 is shown for stagnation pressure and stagnation temperature in Figure 14 and Figure 15, respectively. The overall agreement is satisfying. The largest differences between measurement and calculations can be detected at the hub, where in the boundary layer there is also a great sensitivity to the radial position of the sensor.

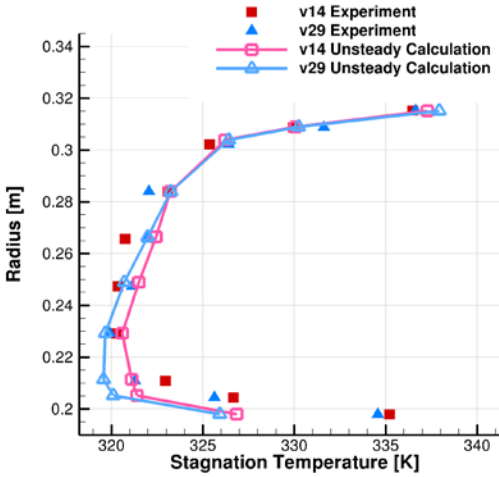

Figure 15 Stagnation temperature at the leading edge of Stator1 for two instrumented vanes

The pressure distribution around the blade is taken as the pressure distribution on the pressure side of vane 23 and the suction side of vane 24. The pressure distribution in time average therefore is composed of two vanes to fit the instrumentation. Of course, it is clear that the probes and time average solution give the same results in the time-domain calculation, but also the agreement with the frequency-domain calculation and the experiments is good. Furthermore, it can be seen that the inclusion of additional modes in the extended HB setup has improved the agreement with the experimental and time-domain results.

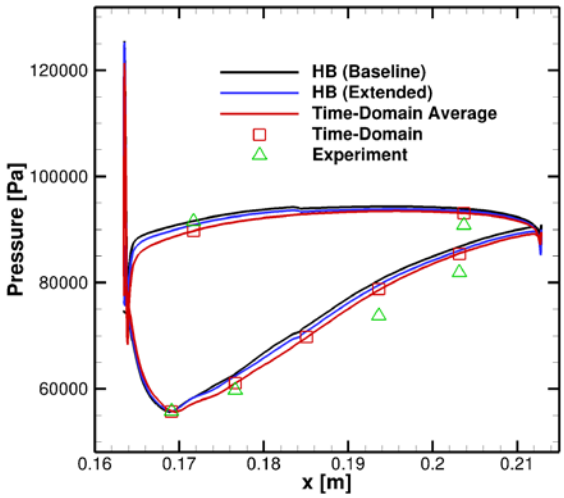

Figure 16 Pressure distribution around Stator1

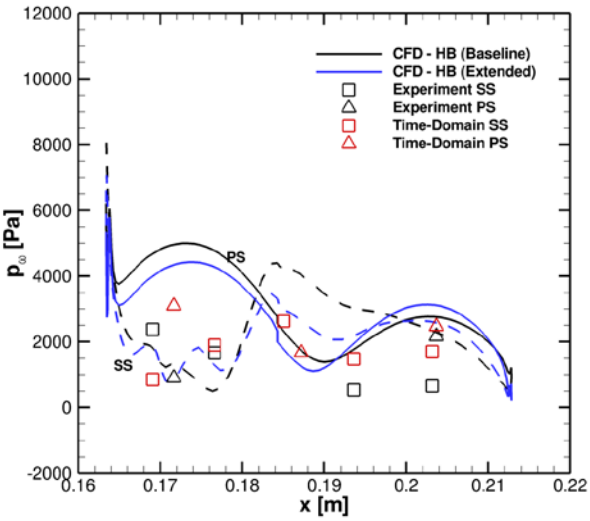

Figure 17 Amplitudes of the Rotor1 BPF

The comparison of the two main frequencies in the spectra of the experiment, the time-domain and the frequency-domain calculations for Rotor1 and Rotor2 BPF are shown in Figure 17 and Figure 18. For the full annulus calculation the available signal of the probes was 1.4 revolutions of which for the DFT only the first period was used in order to obtain pressure amplitudes at the BPFs of Rotor1 and Rotor2. The experimental data was divided into sample lengths of 1 revolution for each of which a DFT was performed. The shown pressure amplitudes are the average of these over 4000 DFTs. As the HB calculation uses only distinct frequencies a comparison with this method should also only use rather few frequencies. By this procedure the experimental frequencies are very close to the interesting frequencies, which for example can occur by slight changes in geometry from blade to blade, can be summarized into the main frequency. For BPF Rotor1 the levels for experimental, time-domain and HB values are closer on the suction side than on the pressure side. The trends are in agreement except for the experimental pressure side. For BPF Rotor2 (Figure 18) the overall agreement is good, except for the experimental pressure side. Due to the stronger up-wind effect of Rotor2 compared to the downwind effect of the wakes of Rotor1 all levels of pressure amplitudes are higher. Comparing the results of the baseline and extended HB simulations it can be seen that the largest differences are observed in the pressure amplitudes at the BPF of Rotor1. In general there are two possible reasons for these differences. Firstly, the coupling of the addition modes with the time-mean flow can alter the underlying flow and therefore impact indirectly the amplitude of the pressure fluctuations. Or, secondly, the additional modes may represent directly the pressure fluctuations at the frequency of interest. For the pressure disturbances at the BPF of Rotor1 both mechanisms are possible. For the pressure disturbances at the BPF of Rotor2 only the former is possible since no additional modes describing this frequency were included in the extended setup. It is therefore reasoned that the larger changes at the BPF of Rotor1 are due to the additional mode at this frequency. Generally, again, it can be seen that the inclusion of addition modes improves the degree of agreement with the time-domain and experimental data.

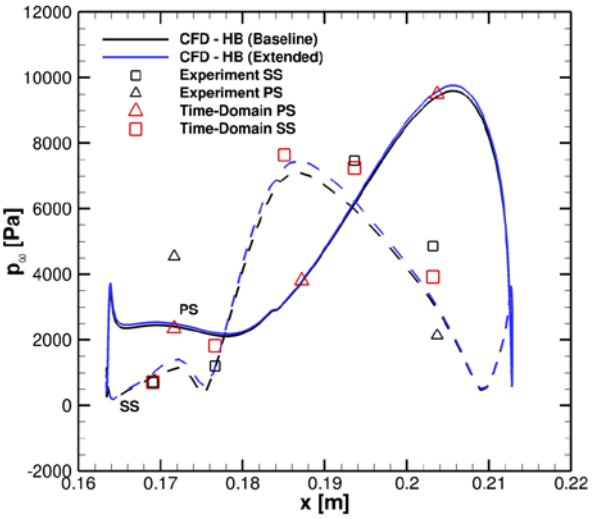

Figure 18 Amplitudes of the Rotor2 BPF

CONCLUSIONS

The calculations show an acceptable agreement between experiment, full annulus calculations in the time-domain and frequency-domain calculations.

As the full annulus calculations are very time consuming and have a high computational cost, it should always be considered, if it is not possible to use frequency-domain calculations for the case being studied.

Although the costs of the time-domain simulations are high, such simulations remain important since, as the results here demonstrate, it is not always possible to capture all effects, at least efficiently, with frequency-domain methods.

The time-domain calculation could be enhanced by splitting the solution and the mesh in different files to save disk space. Also a flexible handling of probe locations and the possibility of adding or modifying these during calculations without the need to stop and restart is desirable.

Furthermore as the saving of the complete solution is impracticable due to the large amount of data and the capacity to do post-processing the code should be capable of defining either fixed spaces or rotating spaces as probe locations to be comparable to the different possibilities of experimental probing.

Altogether new capabilities in computing and enhanced methods of solving the Navier-Stokes-Equations also in the frequency-domain open new insights in the flow in turbo-machinery.

NOMENCLATURE

BDF	Backward difference formula
BPF	Blade passing frequency
CFD	Computational fluid dynamics
D	Diameter [m]
DLR	German Aerospace Center ,German: **D**eutsches Zentrum für **L**uft- und **R**aumfahrt
HB	Harmonic balance
IGV	Inlet guide vane
L	Length [m]
m	Modenumber
M2VP	Multistage two shaft compressor test facility
N	Number of blades/vanes
RAM	Random access memory
RANS	Reynolds Averaged Navier-Stokes
Rig250	4.5 stage DLR research compressor
TRACE	DLR RANS-solver
VPF	Vane passing frequency
ω	Disturbance frequency [Hz]
Ω	Rotational speed [Hz]

ACKNOWLEDGMENTS

The work reported in this paper was conducted within the project PERFEKT, funded by the Bundesministerium für Wirtschaft und Technologie (BMWi) under contract number 20T1309B.

Rolls-Royce Deutschland is gratefully acknowledged for the good collaboration during this project.

REFERENCES

[1] Bardina, J., Ferziger, J. H., and Rogallo, R. S., (1985). Effect of rotation on isotropic turbulence: computation and modelling. Journal of Fluid Mechanics, 154, p. 321336.

[2] Becker, K., Heitkamp, K., and Kügeler, E. (2010). Recent progress in a hybrid-grid CFD solver for turbomachinery flows. V European Conference on Computation Fluid Dynamics ECCOMAS CFD

[3] Franke, M., Röber, T., Kügeler, E., and Ashcroft, G. (2010). Turbulence treatment in steady and unsteady turbomachinery flows. V European Conference on Computation Fluid Dynamics ECCOMAS CFD

[4] Kato, M., and Launder, B. E., (1993). The modeling of turbulent flow around stationary and vibrating square cylinders. 9th Symposium on Turbulent Shear Flows, p. 10.4.110.4.6.

[5] Reutter, O., Ashcroft, G., Nicke, E., Kuegeler, E. (2017). Unsteady Full Annulus Multi-Stage Compressor Calculations – Details on CFD-Experiment Comparison. CEAS Conference Oct., Bukarest

[6] Wilcox, D., (1988). Reassessment of the Scale-Determining Equation for Advanced Turbulence Models. AIAA Journal, Vol. 26, No. 11, November.

[7] Weber, A., and Sauer, M. (2016). PyMesh – Template Documentation. Technical Report DLR-IB-AT-KP-2016-34. German Aerospace Center (DLR), Institute of Propulsion Technology, Linder Hoehe, Cologne, Germany.

[8] Frey, C., Ashcroft, G., Kersken, H., Voigt, C. (2014) A Harmonic Balance Technique for Multistage Turbomachinery Applications. ASME. Turbo Expo: Power for Land, Sea, and Air, Volume 2B: Turbomachinery ():V02BT39A005. doi:10.1115/GT2014-25230.